

ABOUT THE IMPORTANCE OF THE DEFINITION OF REFLECTANCE QUANTITIES - RESULTS OF CASE STUDIES

G. Schaepman-Strub ^{a, b}, T. Painter ^c, S. Huber ^a, S. Dangel ^a, M. E. Schaepman ^d, J. Martonchik ^e, F. Berendse ^b

^a RSL, Dept. of Geography, Univ. of Zurich, 8057 Zurich, Switzerland - gschaep@geo.unizh.ch

^b Nature Conservation and Plant Ecology Group, WUR, 6708 PD Wageningen, The Netherlands

^c National Snow and Ice Data Center, University of Colorado Boulder, Boulder, CO, USA

^d Centre for Geo-Information, WUR, 6700 AA Wageningen, The Netherlands

^e Jet Propulsion Laboratory, California Institute of Technology, Pasadena, CA, USA

KEY WORDS: Terminology, Comparison, Simulation, Accuracy, Vegetation, Snow, MISR

ABSTRACT:

In the remote sensing user community there is a lack of consistency in definitions and properties of reflectance quantities. On one hand, more recent satellite programs such as NASA's MODIS and MISR sensors take into account the directional dimension of the different reflectance products. On the other hand, many published studies still remain unspecific on the reflectance quantities they are based on, or do not follow common definitions. One example is the term 'albedo' assigned to significantly differing products. This fact makes it difficult and confusing to evaluate and compare published results. Our contribution briefly summarizes basic reflectance nomenclature articles. The main aim is to quantify differences of reflectance products to stress the importance of adequate usage of reflectance definitions and quantities. Results from the comparison of directional-hemispherical reflectance versus bihemispherical reflectance and bidirectional reflectance factors versus hemispherical-directional reflectance factors are shown. We exemplify differences of these quantities using modelling results of a black spruce forest canopy and snow cover, as well as selected biome-specific MISR reflectance products of the year 2001.

The presented case studies can only give an insight into the dimension of the problem. The actual differences in the reflectance products of a remotely sensed surface depend on the atmospheric conditions, the surroundings, topography, and the scattering properties of the surface itself. Never the less the presented results are urging the user community to be more specific on the application and definition of reflectance quantities.

1. INTRODUCTION

The Earth-looking remote sensing community increasingly understands the effects of solar illumination geometry and sensor viewing geometry on airborne and satellite data due to the anisotropic reflectance of the Earth's surface and the atmosphere. Not only the direction of illumination and observation influence the measured reflectance, but also their opening angle. Different reflectance quantities have been defined to describe the corresponding conditions of the measurements (Nicodemus, 1977; Martonchik, 2000).

Nevertheless, these conditions are often partly or fully neglected by the user community, and different reflectance quantities are equated, which is especially true for the so-called surface reflectance and albedo (e.g., Breuer, 2003).

The reflectance anisotropy of observed surfaces contains unique information about its structure and the optical properties of the scattering elements. The underlying concept for the characterization of the anisotropy is the bidirectional reflectance distribution function (BRDF). It describes the radiance reflected by a surface as a function of a parallel beam of incident light from a single direction into another direction of the hemisphere. Under natural conditions, i.e. for all field, airborne and spaceborne sensor measurements, the assumption of a single direction of the incident beam does not hold true. Natural light is composed of a direct part, thus uncollided radiation, as well as a diffuse component scattered by the atmosphere, and/ or the surroundings of the observed target. The amount and spectral character of the diffuse light irradiating the observed surface is thus depending on the atmospheric conditions, as well as on the topography and the scattering properties of the surroundings. Previous studies have shown the effects of different atmospheric conditions in simulated

and measured data. The aim of this study is to highlight the differences in reflectance caused by different geometries of the opening angle of the illumination, i.e., directional and hemispherical extent. To get a better impression of the influence of the diffuse component included in the hemispherical extent, different direct to diffuse irradiance scenarios are considered. This modelling approach is performed for a black spruce forest canopy, and a snow cover. Secondly, first results of a comparison between directional and hemispherical reflectance products from the Multi-angle Imaging SpectroRadiometer (MISR) are presented for selected test sites.

This study gives an easy access to the basic concept of reflectance quantities for the user community, by summarizing the nomenclature articles of Nicodemus (1977) and Martonchik (2000). It highlights the importance of a proper usage of definitions through quantitative comparison of different reflectance products.

2. DEFINITIONS

2.1 Radiance, reflectance, reflectance factors

Spectral radiance is the most important quantity to be measured in spectroradiometry. In particular it is *the* quantity required for quantitatively analyzing directional effects. The surface leaving radiance is assumed to be dependent on the incident radiation onto the surface, thus the reflectance is defined as the ratio of reflected to incident flux. Following the concept of energy conservation, its values are in the inclusive interval 0 to 1. The reflectance factor is the ratio of the radiant flux reflected by a surface to that reflected into the same reflected-beam geometry by an ideal (lossless) and diffuse (Lambertian) standard surface,

irradiated under the same conditions. For measurement purposes, a Spectralon panel commonly approximates the ideal diffuse standard surface. Reflectance factors may reach values beyond 1, especially for highly specular reflecting surfaces.

2.2 Geometrical considerations of the incident and reflected fluxes

The basic concept describing the reflectance anisotropy of a surface is the BRDF. Conceptual quantities of reflectance include the assumption that the size/ distance ratio of the illuminating source (usually the sun or lamp) and the observing sensor is assumed to be zero and are usually labelled *directional* in the general terminology. Since infinitesimal elements of solid angle do not include measurable amounts of radiant flux, and unlimited small light sources and sensor field of views do not exist, all *measurable* quantities of reflectance are performed in the *conical* or *hemispherical* domain of geometrical considerations. Thus, actual measurements always involve non-zero intervals of direction and the underlying basic quantity for all radiance and reflectance measurements is the conical case, including the special case of a cone of hemispherical extent. In the case of hemispherical illumination under field conditions, the irradiance can be divided into a direct sunlight component and a second irradiance component scattered by the atmosphere and terrain, which leads to an anisotropic, diffuse sky illumination. Being a function of wavelength, the ratio of diffuse/direct incident irradiance highly influences the spectral dependence of directional effects as shown in the snow case study below.

According to Nicodemus (1977), the angular characteristics of the incoming radiance are named first in the term and are followed by the angular characteristics of the reflected radiance. This leads to the following nomenclature of reflectance quantities (Table 1):

Reflected Incoming	Directional	Conical	Hemispherical
Directional	Bidirectional Case 1	Directional-conical Case 2	Directional-hemispherical Case 3
Conical	Conical-directional Case 4	Biconical Case 5	Conical-hemispherical Case 6
Hemispherical	Hemispherical-directional Case 7	Hemispherical-conical Case 8	Bi-hemispherical Case 9

Table 1: Relation of incoming and reflected radiance terminology used to describe reflectance quantities. The labelling with 'Case' corresponds to Nicodemus (1977). Grey fields correspond to measurable quantities, whereas the others denote conceptual quantities.

2.3 Examples for measurable quantities and derived products

Referring to Table 1, typical measurement instrumentation with resulting reflectance products can be listed for the individual cases. The biconical reflectance (Case 5) is a typical laboratory setup, where a collimated light source illuminates a target that is measured using a non-imaging spectroradiometer. A special case is the conical-hemispherical reflectance (Case 6), where in the laboratory

the sensor is replaced using a cosine receptor for hemispherical measurement. The hemispherical-conical reflectance (Case 8) corresponds to the most common measurement of satellites or airborne and field instruments (e.g., MERIS, ASD FieldSpec). Finally, bi-hemispherical reflectance (Case 9) is measured using albedometers.

Even though measurable quantities only reflect Cases 5, 6, 8 and 9 in Table 1 above, the non-zero interval of the sensor's field of view may be neglected and resulting quantities are reported as being bidirectional or hemispherical-directional measurements. Most satellite reflectance products delivered after atmospheric correction procedures are labelled 'surface reflectance' (e.g., MODIS (Vermote, 1999)). Nevertheless, in many cases the underlying concept of the used reflectance nomenclature is unclear or undocumented, resulting in significant difficulties to assign the proper terminology to the delivered data product. As long as data from satellite or airborne sensors and field spectrometers are not corrected for the hemispherical angular extent of the incoming radiance, the reflected measured quantity always depends on the actual direct and diffuse components of the irradiance over the whole hemisphere. As a consequence, data without a proper specification of the corresponding beam geometries are subject to misinterpretation and subsequently lead to larger uncertainties.

Table 2 shows typical reflectance products and their derivation from the satellite measurement. The integration of the HDRF (Case 7) over the viewing hemisphere results in the BHR (Case 9). Using a modelling approach (e.g., Martonchik 1994; Lyapustin, 1999), the HDRF data (Case 7) is further used to derive BRF (Case 1), and finally, DHR (Case 3) can be derived from BRF (Case 1) by hemispherical integration over the viewing hemisphere. A special case is the derivation of the BRDF from the BRF (again Case 1), which is simply scaling the BRF by $1/\pi$.

Measurement	Derived Products		
Hemispherical-Conical Reflectance Case 8	HDRF Hemispherical-Directional Reflectance Factor Case 7	BRF Bidirectional Reflectance Factor Case 1	BRDF Bidirectional Reflectance Distribution Function Case 1
			DHR Directional-Hemispherical Reflectance Case 3
		BHR Bi-hemispherical Reflectance Case 9	

Table 2: Conceptual data processing chain of airborne and satellite measurements. The table is read from the left to the right side.

The abovementioned derivations of conceptual reflectance quantities from measured reflectance data include the application of a BRDF model. Thus, derived conceptual quantities depend not only on the sampling scheme, availability and accuracy of measured data, but also on the model itself.

3. CASE STUDIES COMPARING DIFFERENT REFLECTANCE QUANTITIES

The following case studies highlight differences of the above described reflectance quantities using model simulations for a vegetation canopy, and a snow surface, as well as MISR data products for several scenes. The differences of hemispherical versus directional reflectance quantities (i.e., BHR (Case 9) versus DHR (Case 3) and HDRF (Case 7) versus BRF (Case1)) are computed for different wavelengths regions and various ratios of direct to diffuse illumination.

We concentrate on reflectance and reflectance factor quantities. Deriving the bidirectional reflectance distribution function from HDRF measurements without correcting for the diffuse illumination, leads to severe distortions of the resulting function (Lyapustin, 1999).

3.1 Vegetation canopy reflectance simulations using the RPV model

3.1.1 Methods and data: Using the PARABOLA instrument, black spruce forest HDRF data were acquired at eight solar zenith angles (35.1°, 40.2°, 45.2°, 50.2°, 55.0°, 59.5°, 65.0°, 70.0°) (Deering, 1995). After applying a simple HDRF to BRF atmospheric correction scheme, data of the red band (650 to 670nm) were fitted to the parametric Rahman-Pinty-Verstraete (RPV) model (Engelsen, 1996). Resulting fit parameters and the RPV are used to simulate different reflectance quantities of a black spruce canopy under various illumination conditions. The model was run for a solar zenith angle of 30° and increments of direct (d) and diffuse irradiance of $d=1.0$, $d=0.8$, $d=0.6$, $d=0.4$, $d=0.2$, and $d=0.0$. These irradiance scenarios corresponded to BRF ($d=1.0$) and HDRF for the rest, including the special case of white-sky HDRF, i.e. purely diffuse irradiance ($d=0.0$).

3.1.2 Results: Figure 1 (top) reports the HDRF of black spruce for indicated direct-diffuse ratios in the solar principal plane, assuming the incident diffuse radiation to be isotropic. The wavelength range is 650 to 670 nm. As is expected for a vegetation canopy, there is a large amount of backscattering, and a hot spot at view zenith 30° due to the lack of shadowing. For d approaching 0, the anisotropy is smoothed and the hot spot becomes invisible.

Fig. 1 (centre) reports the DHR of black spruce as a function of the illumination zenith angle. As previously described for vegetation, the DHR increases with increasing illumination zenith (Kimes, 1983). For comparison, the white-sky BHR (although not a function of any angle) is plotted. The actual albedo can be expressed as a combination of DHR and white-sky BHR if the diffuse incident radiation is assumed to be isotropic. The actual albedo for a given illumination zenith angle then lies on a vertical line between the DHR and white-sky BHR as shown in the graph for an example of 20° solar zenith.

Finally, Figure 1 (bottom) reports the BRF at nadir view as a function of the illumination zenith angle, along with the white-sky HDRF at nadir view (although not a function of any illumination angle).

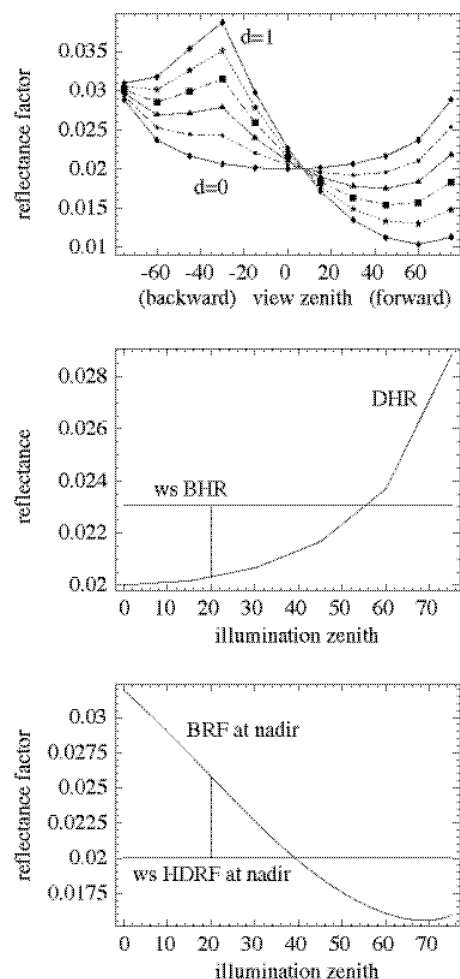


Figure 1. Simulated BRF data for a black spruce canopy in the solar principal plane, and corresponding HDRF for varying direct to diffuse irradiance conditions (top), DHR, and BHR for pure diffuse illumination as a reference (centre), BRF at nadir, and HDRF at nadir for pure diffuse illumination (bottom).

3.2 Snow reflectance simulations

3.2.1 Methods and data: This case study presents model results from a snow directional reflectance model. The model is the coupling of single-scattering parameters and a discrete-ordinates multiple scattering model. Single-scattering parameters were determined with a ray-tracing model for spheroidal particles (Macke, 1996) and the multiple scattering calculations were performed with the DISORT model (Stamnes, 1988).

The single-scattering parameters used in the model were the single-scattering albedo, extinction efficiency, and the single-scattering phase function. Model results shown here are for a spheroid of minimum and maximum radii of 208 μm and 520 μm , respectively. This spheroid has the same surface area to volume ratio as a sphere of radius 250 μm . We then determined 20 Legendre moments of the single-scattering phase function for input to the multiple scattering model. The multiple scattering model was run for a solar zenith of 30°, illumination scenarios as mentioned for the black spruce canopy, and the wavelength range from 0.4 to 2.5 μm .

3.2.2 Results: In Figure 2, we show resulting BRF and HDRF data in the solar principle plane.

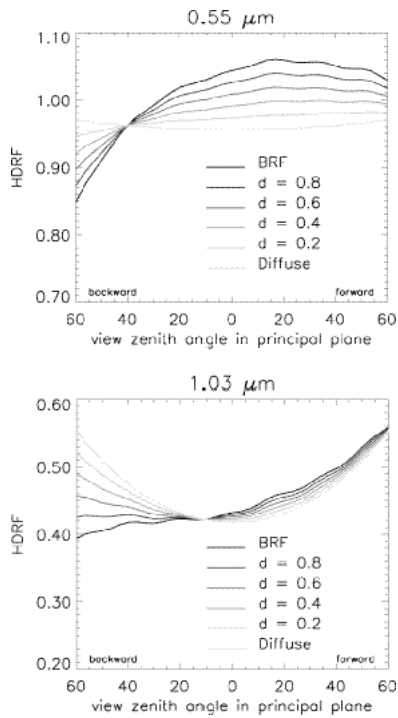


Figure 2. Simulated snow HDRF data for the range of indicated irradiance scenarios, and BRF data in the solar principal plane at $0.55 \mu\text{m}$ (top) and $1.03 \mu\text{m}$ (bottom).

The models for $d = 1.0$ through $d = 0.2$ irradiance exhibit a forward reflectance distribution that decreases in magnitude with increasing diffuse component. For the totally diffuse irradiance scenario, the distribution has a shallow bowl shape. This minimum at nadir results from the angular intersection of the strong forward scattering phase function with the surface. Off-zenith irradiance has a greater chance than zenith irradiance of surviving multiple scatterings due to the orders of magnitude greater single scattering in the forward direction. In other words, zenith irradiance requires far more scattering events to produce reflected radiance than off-zenith. Therefore, the distribution will have greater reflectance at the larger view zenith angles.

The bowl-shaped distribution for diffuse irradiance becomes relatively deeper at longer wavelengths (Figure 2 (bottom)). We show the $1.03 \mu\text{m}$ model because this is the wavelength range in which snow reflectance is most sensitive to grain size (Nolin, 2000; Green, 2002). The enhancement of the bowl shape at greater diffuse irradiance is explained as above coupled with a decrease in the single-scattering albedo at the longer wavelengths. This in turn is due to the increase in the imaginary part k of the complex refractive index at these wavelengths (Warren, 1982). Only for the BRF and $d = 0.8$ irradiance cases is the distribution properly forward reflecting.

Figure 3 shows DHR of snow relative to the illumination zenith angle with the associated white-sky BHR included for reference. For both wavelengths, the DHR increases with increasing zenith angle but the increase is far greater in absolute and relative reflectance for the $1.03 \mu\text{m}$ case. The increase in both cases is due to the change in the angle of the intersection of the single scattering phase function with the surface. The single scattering phase function of ice particles

in the forward angles is several orders of magnitude greater than in the rest of the scattering domain. Therefore, as the illumination zenith angle increases, the forward scattered photons have a higher probability of escaping the snowpack. This in turn increases the albedo of snow.

Because the single scattering albedo of ice particles (in this case a spheroid of radii $208 \mu\text{m}$ and $520 \mu\text{m}$) is 0.9999817 at $0.55 \mu\text{m}$ versus 0.9930210 at $1.03 \mu\text{m}$, multiply scattered photons are more likely to be absorbed at $1.03 \mu\text{m}$. The greater increase in albedo at $1.03 \mu\text{m}$ results then from the increase in the contribution of singly scattered photons to albedo due to the increase in illumination zenith angle. At both wavelengths, the effective illumination zenith angle for white-sky BHR is $49\text{-}50^\circ$, as discussed above.

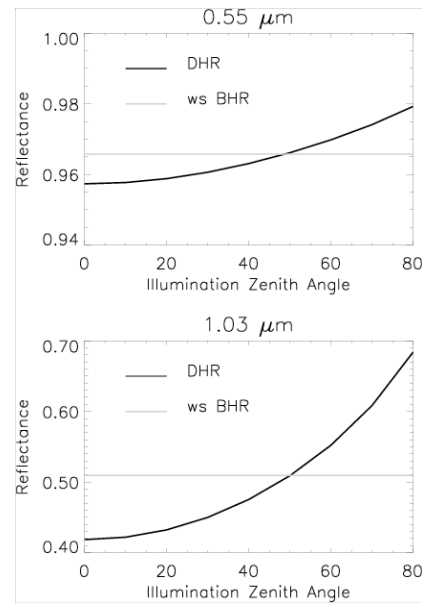


Figure 3. DHR versus illumination zenith angle for snow at $0.55 \mu\text{m}$ (top) and $1.03 \mu\text{m}$ (bottom). The BHR for diffuse illumination (white-sky BHR) is included for comparison.

3.3 Analysis of MISR surface reflectance data products

3.3.1 Methods and selected datasets: Various land surface reflectance products are available from the MISR sensor, launched in 1999. MISR has nine cameras with centre view directions of 26.1 , 45.6 , 60.0 , and 70.5 degrees in forward and afterward direction, as well as one looking in nadir direction. All cameras cover four spectral bands with a centre wavelength at 446 , 558 , 672 , and 867 nm. The crosstrack IFOV and sample spacing of each pixel is 275 m for all of the off-nadir cameras, and 250 m for the nadir camera. Downtrack IFOV's depend on view angle, ranging from 214 m in the nadir to 707 m at the most oblique angle. However, sample spacing in the downtrack direction is 275 m in all cameras (Diner, 1999).

We briefly describe the retrieval of the land surface products HDRF, BHR, BRF, and DHR. For the mathematical formulation refer to Martonchik (1998). The top-of-atmosphere MISR radiances are atmospherically corrected to produce the HDRF and BHR, surface reflectance properties as would be measured at ground level but at the MISR spatial resolution. The MISR surface retrievals do not explicitly incorporate tilt or slope effects (Diner, 1999). The HDRF and BHR then are further atmospherically corrected to remove all

diffuse illumination effects, resulting in the BRF and DHR. The determination of these surface products obviously requires that the atmosphere be sufficiently characterized in order for the correction process to occur. This characterization is accomplished by means of an aerosol retrieval. After a BRF is determined, it is fitted to a three parameter empirical BRF model, which provides a convenient representation of the surface scattering characteristics.

We statistically analyzed the differences of directional and hemispherical MISR reflectance data products, namely DHR versus BHR and BRF versus HDRF. These data products are compared to each other by their respective mean values, mean absolute and relative difference. Additionally, their correlation is derived. For further analysis of the products and their differences, the mean value of the absolute HDRF uncertainty and relative BHR uncertainty product was calculated, as well as the mean aerosol optical depth (AOD) value in the green spectral band of all analyzed pixels.

The ratio of diffuse to direct illumination increases with increasing AOD. Therefore we expect the largest difference between HDRFs and BRFs in shorter wavelength ranges, i.e., in the blue band, where the diffuse component of the illumination is largest. This wavelength dependence is due to the decreasing influences of Rayleigh scattering and aerosols with increasing wavelength.

We selected ten datasets, acquired in 2001, that correspond to MISR data product version 12. For all analyzed data, a comparison of MISR optical depths with those from an included ground based AERONET site showed good correlation in all four MISR spectral bands. The reliability of the land surface reflectance values depends upon the AOD magnitude. Therefore, pixels with an AOD larger 0.5 at 558 nm (green spectral band) have been excluded from the MISR scenes. In the following, all quantities called 'scene-averaged' rely on this exclusion.

The sites were selected to represent different biome types, following the MODIS IGBP land cover map. Three sites are covered twice, under different atmospheric conditions and sun zenith angles (Table 3).

Site	Country	Date 2001	Mean sz [°]	Main biome type (IGBP)	Mean AOD
Howland	Maine, US	07/21	27.7	Mixed f., decid. broadl f.	0.10
Railroad Valley	Nevada, US	08/17	28.4	Barren or sparsely veg.	0.99
Mongu	Zambia	07/11	44.6	Savannas, croplands	0.05
Banizou mbou	Niger	10/04	24.1		0.31
		12/23	41.4		0.11
Hombori	Mali	07/05	19.6		0.36
Avignon	France	07/12	25.2		0.07
		08/29	36.9		0.19
Bordeaux x	France	05/30	24.5	Everg. needlel. f., croplands, mixed forest	0.24
		07/01	24.0		0.12

Table 3. Overview of MISR scenes selected for the analysis of the land surface products.

3.3.2 Results: Differences between BHR (Case 9) and DHR (Case 3)

In general, BHR and DHR product values derived from the MISR sensor are highly correlated, with r^2 values between 0.98 and 1.0 throughout all spectral bands and analyzed

scenes (with the exception of the Hombori scene blue band, where r^2 reaches 0.84 only).

For all analyzed MISR images, the relative scene-averaged difference between BHR and DHR reaches a maximum of 2.7 % of the BHR value (with the exception of the difference in the blue band of the Hombori scene reaching 5.1%) for all four spectral bands (Table 4). Numerically, this is a small difference, compared to the data uncertainties. The lowest scene-averaged relative BHR uncertainty is 5.6% for the NIR spectral band of the Avignon (07/12) scene, whereas relative BHR uncertainty can easily reach values around 20% and much higher, with a maximum of 88% for the blue spectral band of the Banizoumbou (10/04) scene.

As detailed above, we expect a trend of decreasing differences between BHR and DHR with increasing wavelength, thus the blue band reflectances should show the largest relative differences. Results show that the relative reflectance difference of five scenes is biggest in the blue band, whereas for the other 5 cases, differences reach the same or even higher values in at least one of the other bands.

Site	SZ [°]	Mean AOD	Mean BHR Mean ((BHR-DHR)/BHR) [%]			
			446nm	558nm	672nm	867nm
Howland	27.7	0.10	0.031 2.1	0.053 1.5	0.028 1.1	0.318 0.7
Railroad Valley	28.4	0.99	0.095 1.7	0.137 1.3	0.170 0.9	0.238 0.7
Mongu	44.6	0.05	0.046 0.5	0.078 0.3	0.094 0.3	0.246 0.6
Banizou mbou	24.1	0.31	0.060 1.2	0.126 1.5	0.176 1.4	0.357 1.3
	41.4	0.11	0.084 0.5	0.160 0.5	0.261 0.6	0.376 0.6
Hombori	19.6	0.36	0.108 5.1	0.232 2.5	0.349 1.6	0.412 1.2
Avignon	25.2	0.07	0.045 2.0	0.075 1.4	0.069 0.9	0.307 0.8
	36.9	0.19	0.050 0.9	0.081 0.9	0.079 0.7	0.286 0.8
Bordeaux	24.5	0.24	0.059 1.5	0.097 2.0	0.087 1.4	0.320 1.2
	24.0	0.12	0.048 1.8	0.078 1.5	0.073 1.0	0.304 0.9

Table 4. Comparison of BHR and DHR values for the selected MISR scenes.

Differences between the BHR and DHR product can be related to the actual aerosol optical depth in the green spectral band. This relation is weak for the BHR-DHR differences in the blue band ($r^2 = 0.29$) and gets much stronger with increasing wavelengths, with a maximum for the NIR region ($r^2 = 0.79$).

Differences between HDRF (Case 7) and BRF (Case 1)

As with the results for the hemispherical reflectances, the relationship between HDRF and BRF values show a high correlation, with r^2 values above 0.98 throughout all spectral bands, and view angles of all scenes (with the exception of the Hombori scene blue band reflectance reaching an r^2 of 0.67 only).

Compared to the quantities integrated over an extrapolation of the view hemisphere, the relative differences of the reflectances of the single view angles are larger and reach up to 10% of the HDRF value (with the exception of the Hombori scene blue band reflectance difference of 14.2%).

The trend of decreasing differences with increasing wavelength is much stronger for the directional quantities than for the hemispherically integrated quantities. Thus, the

largest relative differences were mostly found in the blue spectral band, with very few exceptions.

Comparing the relative HDRF-BRF differences with regard to the viewing direction, there is a clear trend of higher differences for the forward looking camera. Further we investigated the relative differences of the HDRF-BRF values with regard to the nine cameras. For most scenes and spectral bands, the Ba camera (view zenith of 45.6°) shows the smallest differences. This indicates, that whenever the hemispherical irradiance component is neglected and HDRF data are equated with BRF data, the introduced uncertainties can be reduced by applying off-nadir data in the backward scattering direction, instead of nadir data.

4. CONCLUSION

All remote sensing data depend on the illumination and view geometry of the sensor, as well as on their opening angle. Different reflectance quantities have been defined to describe the corresponding conditions of the measurements. The basis for the proper use of these reflectance quantities is a standardized nomenclature, well known throughout the remote sensing community. This study summarized the nomenclature articles of Nicodemus (1977) and Martonchik (2000) to give an easy access to the concept.

Further the importance of using the adequate reflectance product is shown. All reflectance measurements performed under natural conditions include a diffuse fraction. Its amount is a function of the atmospheric conditions, the topography, the surroundings of the observed surface, and the wavelength. It thus introduces spectral effects to spectrometer data. The presented case studies are concentrating on the opening angle of the illumination, restricting it to directional irradiance only, or allowing for a diffuse irradiance component. The effect of varying direct to diffuse irradiance ratio is significant in modelled data, as well as in analysed MISR reflectance products.

This study is addressing different remote sensing communities. It shows that the use of any remote sensing data has to include the analysis of the corresponding illumination and view geometry, and the opening angle, as a prerequisite for any further analysis. This will explain many unexpected results and significantly reduce uncertainties. Some satellite products of the MODIS and MISR sensor account for these considerations. It is the responsibility of the users to choose for the adequate product, guided by the reflectance nomenclature. Further, state of the art models allow users to account for the anisotropy of the target and the illumination conditions.

The publication shall motivate the remote sensing community to take reflectance nomenclature into account and use the presented common basis for the sake of clarification and comparability. Even though not all applications of remote sensing data take the directionality of the reflectance signal into account, the appropriate selection and denomination of the used reflectance quantity is a prerequisite for every scientific publication.

5. ACKNOWLEDGEMENT

This work was supported by the Swiss National Science Foundation, under contract 200020-101517. MISR data were obtained from the NASA Langley Research Center Atmospheric Sciences Data Center.

6. REFERENCE

Breuer, L., K. Eckhardt, H. Frede, Plant parameter values for models in temperate climates, *Ecol Model*, 169 (2-3), 237-293, 2003.

Deering, D., S. Ahmad, T. Eck, B. Banerjee, Temporal Attributes of the Bidirectional Reflectance for three Boreal forest canopies, *IGARSS*, pp. 1239-1241, Florence, Italy, 1995.

Diner, D., J. Martonchik, C. Borel, S. Gerstl, H. Gordon, Y. Knyazikhin, R. Myneni, B. Pinty, M. Verstraete, Multi-angle Imaging Spectro-Radiometer Level 2 Surface Retrieval Algorithm Theoretical Basis, JPL D-11401, Rev. D, December 2, 1999, JPL, California Institute of Technology, 1999.

Engelsen, O., B. Pinty, M. Verstraete, J. Martonchik, Parametric bidirectional reflectance factor models: evaluation, improvements and applications, pp. 114, EC JRC, Ispra, Italy, 1996.

Green, R., J. Dozier, D. Roberts, T. Painter, Spectral snow-reflectance models for grain-size and liquid-water fraction in melting snow for the solar-reflected spectrum, *Ann Glaciol*, 34, 2002, 34, 71-73, 2002.

Kimes, D., Dynamics of Directional Reflectance Factor Distributions for Vegetation Canopies, *Appl Optics*, 22 (9), 1364-1372, 1983.

Lyapustin, A., J. Privette, A new method of retrieving surface bidirectional reflectance from ground measurements: Atmospheric sensitivity study, *J Geophys Res-Atmos*, 104 (D6), 6257-6268, 1999.

Macke, A., M. Mishchenko, Applicability of regular particle shapes in light scattering calculations for atmospheric ice particles, *Appl Optics*, 35 (21), 4291-4296, 1996.

Martonchik, J., Retrieval of Surface Directional Reflectance Properties Using Ground-Level Multiangle Measurements, *Remote Sens Environ*, 50 (3), 303-316, 1994.

Martonchik, J.V., D.J. Diner, B. Pinty, M.M. Verstraete, R.B. Myneni, Y. Knyazikhin, and H.R. Gordon, Determination of land and ocean reflective, radiative, and biophysical properties using multiangle imaging, *Ieee T Geosci Remote*, 36 (4), 1266-1281, 1998.

Martonchik, J., C. Bruegge, A. Strahler, A review of reflectance nomenclature used in remote sensing, *Remote Sensing Reviews*, 19, 9-20, 2000.

Nicodemus, F., J. Richmond, J. Hsia, I. Ginsberg, T. Limperis, Geometrical Considerations and Nomenclature for Reflectance, NBS, US Department of Commerce, Washington, D.C., 1977.

Nolin, A., J. Dozier, A hyperspectral method for remotely sensing the grain size of snow, *Remote Sens Environ*, 74 (2), 207-216, 2000.

Stamnes, K., S. Tsay, W. Wiscombe, K. Jayaweera, Numerically Stable Algorithm for Discrete-Ordinate-Method Radiative-Transfer in Multiple-Scattering and Emitting Layered Media, *Appl Optics*, 27 (12), 2502-2509, 1988.

Vermote, E., A. Vermeulen, Atmospheric correction algorithm: Spectral reflectances (MOD09), MODIS ATBD, pp. 107, Univ. of Maryland, Dept. of Geography, 1999.

Warren, S., Optical-Properties of Snow, *Rev Geophys*, 20 (1), 67-89, 1982.